Published online April 23, 2004

Nucleic Acids Research, 2004, Vol. 32, No. 7 ***e65***
DOI: 10.1093/nar/gnh065

Monitoring denaturation behaviour and comparative stability of DNA triple helices using oligonucleotide–gold nanoparticle conjugates

Deirdre Murphy, Ramon Eritja[1] and Gareth Redmond*

Nanotechnology Group, NMRC, Lee Maltings, Cork, Ireland and [1]Department of Structural Biology, Instituto de Biología Molecular de Barcelona, CSIC, Jordi Girona 18-26, E-08034 Barcelona, Spain

Received February 6, 2004; Revised March 10, 2004; Accepted March 29, 2004

ABSTRACT

Gold nanoparticle labels, combined with UV-visible optical absorption spectroscopic methods, are employed to probe the temperature-dependent solution properties of DNA triple helices. By using oligonucleotide–nanoparticle conjugates to characterize triplex denaturation, for the first time triplex to duplex melting transitions may be sensitively monitored, with minimal signal interference from duplex to single strand melting, for both parallel and antiparallel triple helices. Further, the comparative sequence-dependent stability of DNA triple helices may also be examined using this approach. Specifically, triplex to duplex melting transitions for triplexes formed using oligonucleotides that incorporate 8-aminoguanine derivatives were successfully monitored and stabilization of both parallel and antiparallel triplexes following 8-aminoguanine substitutions is demonstrated.

INTRODUCTION

There is increasing interest in the design of sequence-specific DNA-binding molecules that may have diagnostic or therapeutic uses (1,2). In this regard, naturally occurring triple helix DNA can be found in living cells and is thought to play a role in DNA transcription, cleavage and recombination (3–5). Also, oligonucleotides may bind oligopurine–oligopyrimidine sequences of double-strand DNA by forming triple helices (triplexes) (6). Depending on the orientation of the third strand with respect to the central oligopurine Watson–Crick strand, triplexes are classified into two main categories: (i) parallel and (ii) antiparallel. Parallel triplexes require protonation of N3 of cytosine to form correct Hoogsteen bonding with N7 of guanine. For this reason parallel triplexes are mostly stable under acidic conditions. In comparison, antiparallel triplexes require no protonation and exhibit pH-independent strong binding. The ability to target specific sequences of DNA through oligonucleotide-based triple helix formation provides a powerful tool for genetic manipulation, suggesting that triplex DNA has potential applications in DNA sequencing, gene control and gene therapy (3–5).

In order for triplex DNA to realize its maximum potential, it is essential to develop novel methods that will permit the characteristics of these structures to be completely elucidated. One of the most common ways to assess the affinity of oligonucleotides for targets, such as triplex-forming double-strand DNA, is the use of melting experiments followed by UV absorbance. In this technique, nucleic acid bases become unstacked during denaturation, causing an increase in absorbance of the solution, a hyperchromic effect (7). Although this technique is simple to use, it suffers from some limitations. Firstly, the absorbance changes are not large and each assay requires a comparatively large amount of material. Secondly, triplexes have two transitions in their melting profiles (triplex to duplex and duplex to single strand); often these transitions overlap and are not easily distinguished. Thirdly, and more specifically, the formation of antiparallel triplexes is accompanied by only small changes in absorbance, making the evaluation of the properties of these structures difficult (8,9). Notably, a technique based on the use of molecular beacons has recently been applied for the characterization of melting of intramolecular triplexes (10).

Gold nanoparticles bearing oligonucleotides were first described in 1996 (11,12). Since then, these oligonucleotide–nanoparticle conjugates have been used as a means to monitor oligonucleotide hybridization and denaturation, to form networked arrays (11,13,14) and to form predetermined dimeric and trimeric assemblies (12,15). In particular, the optical properties of gold nanoparticles linked to oligonucleotides has attracted large interest due to their potential use in genetic analysis (16–21). In this paper, we characterize the solution phase thermal denaturation processes of 3-dimensional oligonucleotide-linked gold nanoparticle networks, the assembly of which is mediated by oligonucleotide triplex formation, using UV-visible absorbance spectroscopy. In particular, we report for the first time the use of gold nanoparticle labels to accurately monitor the melting behaviour and comparative stability of both parallel and antiparallel DNA triplexes.

MATERIALS AND METHODS

Materials

The following materials were obtained from Sigma-Aldrich (UK): $HAuCl_4$, trisodium citrate dihydrate, citric acid,

*To whom correspondence should be addressed. Tel: +353 21 4904077; Fax: +353 21 4270271; Email: gareth.redmond@nmrc.ie

Na_2HPO_4, NaCl, dithiothreitol (DTT), HCl and HNO_2. NAP-10 columns were purchased from Amersham Pharmacia Biotech (UK). The Gelman 0.45 μm Nylaflo® nylon membrane filters were purchased from Sigma-Aldrich (UK). Nanopure H_2O (18.2 MΩ) purified using an Elgastat Prima purification system was employed during all experiments. All glassware involved in the synthesis of Au nanoparticles was washed first with Aqua Regia (3 HCl:1 HNO_3) and then rinsed thoroughly with deionized water. The nanoparticle solutions were centrifuged using an Eppendorf 5415D microcentrifuge.

Preparation of Au nanoparticles

Au nanoparticles were prepared by the citrate reduction of $HAuCl_4$ (22,23) as follows. An aliquot of 50 ml of aqueous $HAuCl_4$ solution (19.7 mg, 1.0 mM) was heated at reflux and stirred vigorously. An aliquot of 5 ml of aqueous sodium citrate solution (57.04 mg, 38.8 mM) was added rapidly and the reaction went through a colour change from yellow to clear, then to black and finally red within the first minute. The solution was stirred at reflux for a further 15 min, allowed to cool to room temperature and was then filtered under vacuum through a Gelman 0.45 μm Nylaflo® nylon membrane filter to yield a red solution. The resulting nanoparticle sol was analyzed by UV-visible absorption spectroscopy using an Agilent 8453 spectrophotometer. Optical absorbance at 520 nm was recorded and the concentration of the solution was determined using Beer's Law to be 15.66 nM. Transmission electron microscopy, using a JEOL JEM 1200-EX transmission electron microscope, was performed to determine the size distribution of the nanoparticles in the sol.

Preparation of oligonucleotides

Oligonucleotide sequences were synthesized on an Applied Biosystems DNA synthesizer, model 392. Sequences were prepared using standard (Bz- or ibu-protected) 3′-phosphoramidites and bis-DMF-protected 8-aminodeoxyguanine phosphoramidite (24,25). The latter phosphoramidite is now commercially available (Glen Research). Standard 1 μmol scale synthesis cycles were used. Oligonucleotides carrying thiol groups at the 5′-end were prepared using the phosphoramidite of DMT-protected 6-hydroxyhexyl disulfide. Oligonucleotides carrying thiol groups at the 3′-end were prepared using a controlled pore glass (CPG) support functionalized with DMT-protected 3-hydroxypropyl disulfide (Glen Research). Coupling efficiencies were >98%. After synthesis, oligonucleotide supports carrying thiol groups were treated overnight with 1 ml of 50 mM DTT in concentrated NH_3 at 55°C. The support corresponding to the oligonucleotide carrying 8-aminoguanine and a thiol group was treated with 1 ml of concentrated NH_3 containing 0.1 M 2-mercaptoethanol at 55°C for 24 h (25). The resulting solutions were concentrated to dryness. Oligonucleotides bearing thiol groups shall be referred to herein as unmodified oligonucleotides, as distinct from those that have Au nanoparticle labels or those incorporating 8-aminoguanine groups.

Dithiol linkages in thiolated oligonucleotide solutions were cleaved prior to use by adding an appropriate amount of a 0.1 M solution of DTT in 0.17 M sodium phosphate buffer (pH 8). Typically, 20 μl of DTT solution was added to 100 μl of a 100 pmol/μl solution of the oligonucleotide. The solution was allowed to stand at room temperature for 0.5 h. The thiolated oligonucleotides were then desalted on a NAP-10 (Pharmacia) column using a 0.1 M citrate:phosphate buffer (pH 7) as solvent. The resulting fractions were analyzed by UV-visible absorption spectroscopy and the optical absorbance at 260 nm was recorded for each fraction. The optical absorbance at 260 nm of the fraction containing the purified oligonucleotide was used in conjunction with the known extinction coefficient of the oligonucleotide to determine the oligonucleotide concentration according to Beer's Law. Oligonucleotides were prepared for melting experiments by dissolving them at an appropriate concentration in buffer solution (1 M NaCl, 0.1 M citrate:phosphate buffer, pH 7). Oligonucleotide complexes were prepared by mixing 1.5 nmol each strand in a total reaction volume of 1 ml. For reactions at pH 5.5, the pH of the solutions was lowered by the addition of 350 μl of 0.05 M citric acid solution. The solutions were then heated to 90°C for 5 min, slowly cooled to room temperature and left to hybridize for 24 h.

Preparation of oligonucleotide–nanoparticle conjugates

Solutions of Au nanoparticles and oligonucleotides were mixed in appropriate amounts (26), i.e. 2.63 nmol oligonucleotide/ml gold nanoparticles (nanoparticle concentration 15.66 nM) was used. The entire solution was then brought to 0.1 M citrate:phosphate buffer (pH 7). The amounts of reagents used in each conjugate synthesis included a 1.5 molar excess of oligonucleotide. The solution was then shaken for 48 h at 75 r.p.m. on a Heidolph Rotamax 120 shaker. During this time the NaCl concentration of the solution was slowly brought to 0.1 M by the addition of small amounts of a 1 M NaCl, 0.1 M citrate:phosphate buffer (pH 7) solution four times during the 48 h. After 48 h the solution was centrifuged at 13 200 r.p.m. for 30 min. The supernatant was removed and the reddish solid at the bottom of the centrifuge tube was dispersed in 0.1 M NaCl, 0.1 M citrate:phosphate buffer (pH 7) solution (the volume added was similar to that removed). This procedure was repeated and the reddish solid at the bottom was dispersed in 0.3 M NaCl, 0.1 M citrate:phosphate buffer (pH 7). The solution was analyzed by UV-visible spectroscopy and absorbances at 260 and 520 nm were recorded. The concentration of the solution was determined using the absorbance of the solution at 520 nm and Beer's Law (26). The solution was stored at room temperature. Melting experiments were carried out using 2 pmol amounts of each oligonucleotide–gold nanoparticle conjugate (i.e. 0.32 nmol attached oligonucleotides) (27) in 1 M NaCl, 0.1 M citrate:phosphate buffer (pH 7 or 5.5) in a total reaction volume of 1 ml. The solution was heated to 90°C for 5 min, slowly cooled to room temperature and then left to hybridize for 24 h.

Temperature-dependent UV-visible absorption spectroscopy

Optical melting curves were collected on an Agilent 8453 spectrophotometer equipped with an Agilent temperature controlling Peltier unit. The prehybridized solution was transferred to a stoppered 1 cm path length cuvette and UV-visible optical absorption spectra were recorded at 2°C intervals, with a 1–2 min heating time and a hold time of 1 min at each temperature interval, while the sample was heated from 20 to 90°C. The data were collected as

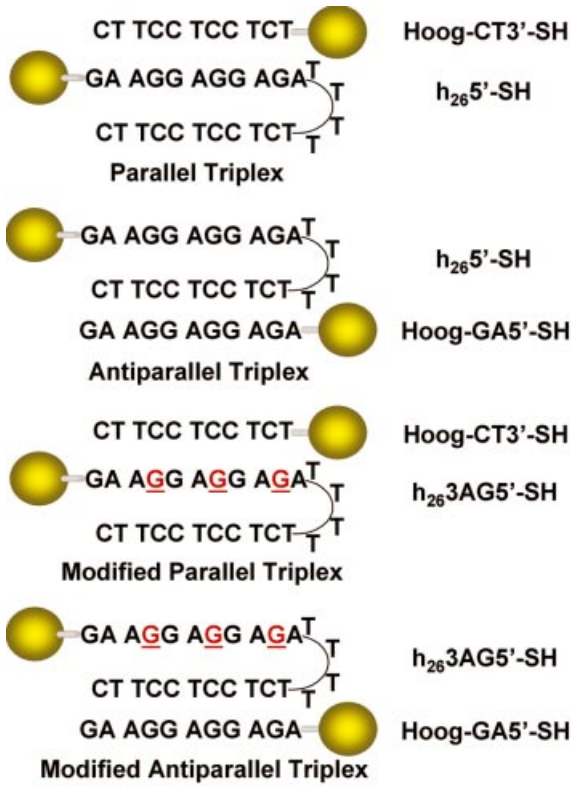

Figure 1. Schematic representation of the various triplex–nanoparticle conjugates investigated in this study. **G**, 8-aminoguanine substitution.

wavelength versus absorbance spectra from which plots of absorbance versus temperature at 260 nm were extracted. The melting temperature of each of the systems was determined from these graphs by plotting the second derivative of each melting curve and finding the point at which each curve crossed the *x*-axis. Melting curves were acquired for several heating and cooling gradients. The apparent T_m obtained using the present method may be overestimated with respect to the T_m obtained under equilibrium by a maximum of up to 1°C.

RESULTS AND DISCUSSION

To explore the use of oligonucleotide–gold nanoparticle conjugates in monitoring triplex denaturation, several parallel and antiparallel triplex-forming oligonucleotides, carrying thiol groups, having the same hairpin duplex as the target (28) were studied (see Fig. 1). As described in Materials and Methods, sequence h_{26}5′-SH (5′-thiol-hexyl-GAAGG-AGGAGA-TTTT-TCTCCTCCTTC-3′), sequence Hoog-CT3′-SH (5′-CTTCCTCCTCT-propyl-thiol 3′) and sequence Hoog-GA5′-SH (5′-thiol-hexyl-AGAGGAGGAAG-3′) were synthesized using the phosphoramidite of DMT-protected 6-hydroxyhexyl disulfide and a CPG support functionalized with DMT-protected 3-hydroxypropyl disulfide. To make oligonucleotide–nanoparticle conjugates, the thiol-terminated oligonucleotides were reacted with citrate-stabilized gold nanoparticles (13 nm) in buffered aqueous solution to obtain a dispersion of gold nanoparticles bearing multiple oligonucleotide molecules per nanoparticle (11).

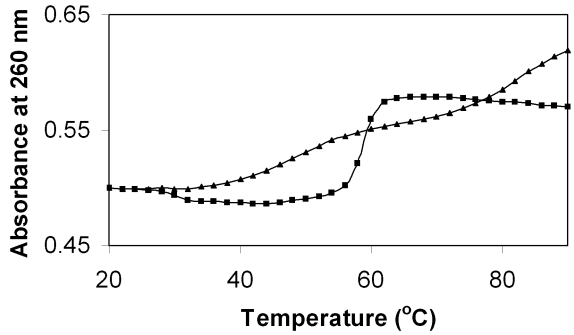

Figure 2. Normalized thermal dissociation curves for (black triangle) unmodified parallel triplexes formed using the hairpin h_{26}5′-SH and the oligonucleotide Hoog–CT3′-SH and for (black square) parallel triplex–nanoparticle aggregates formed using oligonucleotide–nanoparticle conjugates based on the same sequences.

The denaturation behaviour of parallel triplexes formed using unmodified oligonucleotides and oligonucleotide–gold nanoparticle conjugates, respectively, was first investigated. The sequences h_{26}5′-SH and Hoog-CT3′-SH were mixed together in an aqueous citrate:phosphate buffer at pH 5.5. At this pH these sequences hybridize to form parallel triplexes. Denaturation of these triplexes was achieved by slow and steady heating of the hybridized solution. During denaturation, UV-visible absorption spectra of the solution were obtained at 2°C intervals and the melting curve, i.e. the change in the absorbance at 260 nm with respect to temperature, was plotted (see Fig. 2). Two transitions are observed on the melting curve. The first, having a T_m value between 40 and 50°C, is due to the triplex to duplex transition and the second, at ~85°C, is the duplex to random coil transition.

Following this, the melting properties of triplexes formed using strands of identical sequence and modified with gold nanoparticles were investigated. The oligonucleotide–nanoparticle conjugates were first mixed together using the same hybridization solution type and conditions as employed above. Oligonucleotide hybridization results in the formation of 3-dimensional interlinked networks of nanoparticles, referred to as triplex–nanoparticle aggregates. During the hybridization process the solution changes from an initial red colour to a pale blue/black colour. Specifically, significant spectral changes occur in the UV-visible absorption spectra of these solutions at 260 and 520 nm and in the region 600–700 nm due to the formation of nanoparticle aggregates following hybridization of the covalently attached oligonucleotides. These large absorbance changes, as compared with unmodified oligonucleotides, are a result of the marked sensitivity of nanoparticle optical properties to the reduced internanoparticle distances that occur when the nanoparticles are brought into close proximity following hybridization (16–21). The magnitude and reversibility of these spectral changes allows the progress of triplex formation and subsequent denaturation to be monitored optically for very small oligonucleotide concentrations.

To compare the denaturation behaviour of these parallel triplex–nanoparticle aggregates to that of the parallel triplexes formed using unmodified oligonucleotides described above, the solution was heated at 2°C intervals and the change in the absorbance of the solution at 260 nm was measured with

respect to temperature. The derived melting curve shows only one transition, at ~60°C, the triplex to duplex transition (see Fig. 2). As the triplexes denature, the duplex hairpin and single oligonucleotide strands separate and hence the crosslinked nanoparticles also become separated and redisperse into solution, causing a reversal of the spectral changes that occurred during hybridization. Thus this 'melting' transition represents the breakdown of the 3-dimensional interlinked gold nanoparticle networks following triplex denaturation. However, while during heating some of the DNA crosslinks in an aggregate can dissociate without dispersing the Au nanoparticles into solution, every DNA crosslink must dissociate before the nanoparticles can move apart. Hence, the observed optical 'melting' signal, which reflects the average internanoparticle spacing, typically occurs at a higher temperature and over a narrower temperature range than that observed for unmodified strand melting. This sharp 'melting' in triplex–nanoparticle aggregates as compared with melting of unmodified triplexes therefore derives from: (i) a cooperative effect due to the multiple oligonucleotide interconnects between particles in the network structure; (ii) the monitoring of a nanoparticle optical signature that is sensitive to internanoparticle distance and particle aggregate size rather than a DNA nucleotide base signature (16–21). Consequently, while the extraction of formal thermodynamic data from triplex–nanoparticle aggregate melting profiles may be complex, comparative sequence-dependent analysis of aggregate melting offers a convenient way to assess the relative stability of different triplexes. Also, since the hyperchromic change associated with melting of triplex–nanoparticle conjugates (i.e. the triplex to duplex transition) is higher than that of corresponding unmodified triplexes, the subsequent duplex to random coil transition is not observed in these systems as it is accompanied by a comparatively smaller absorbance change.

Antiparallel triplexes formed using unmodified oligonucleotides were prepared in an analogous manner using the same hairpin sequence, h_{26}5′-SH, and a different oligonucleotide sequence, Hoog-GA5′-SH (see Fig. 1). Both unmodified triplexes and triplex–nanoparticle aggregates were then formed. The main difference between parallel and antiparallel triplexes is that parallel triplexes form only at pH 5.5, while antiparallel triplex formation is pH independent (pH 7 used herein). The melting curves obtained from the UV-visible analysis of denaturation of both unmodified triplexes and triplex–nanoparticle aggregates are shown in Figure 3. The melting curve of unmodified triplexes shows a single transition (with a T_m of ~85°C), the duplex to single strand transition. This transition is weak and difficult to determine with accuracy due to the small absorbance change that occurs over a broad temperature range. The triplex to double strand transition is not observed at all, since the purine third strand is largely stacked in the free state (29). Thus, UV-visible absorption spectroscopy cannot be used to determine the melting transition of antiparallel triplexes. For this reason little structural information is available concerning antiparallel triplexes (30–32). This is a pertinent problem given that these triplexes are of widespread interest since they are formed at physiological pH. Other techniques for analysis of antiparallel triplex denaturation have been developed, but these are often more complex and time consuming than the comparatively simple UV-visible monitoring technique. In this regard, we

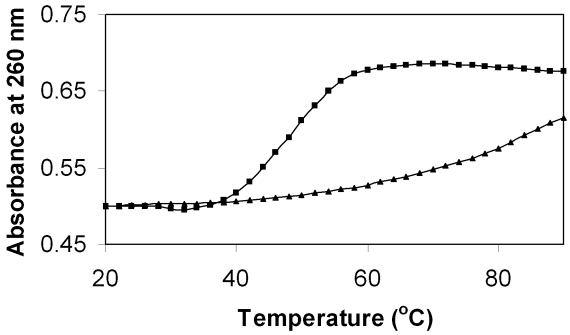

Figure 3. Normalized thermal dissociation curves for (black triangle) unmodified antiparallel triplexes formed from the hairpin h_{26}5′-SH and the oligonucleotide Hoog–GA5′-SH and for (black square) antiparallel triplex–nanoparticle aggregates formed using oligonucleotide–nanoparticle conjugates based on the same sequences.

have recently obtained a value for the T_m of this antiparallel triplex to duplex transition using a more complex multivariate analysis technique (44°C at 10 mM sodium phosphate, pH 4–8) (33).

In comparison, the melting curve of the antiparallel triplex–nanoparticle aggregates shows a single transition that is due to the triplex to duplex transition (see Fig. 3). This transition is strong and well defined for these triplex–nanoparticle aggregates, whereas it is completely undetectable for the same sequences in the absence of gold nanoparticle labels. The duplex to random coil transition is not observed, similar to the results presented above for parallel triplexes. An aggregate 'T_m' value of ~50°C is higher than that measured for unmodified triplexes using multivariate analysis (44°C) (33), consistent with the known melting behaviour of oligonucleotide–nanoparticle aggregates outlined above. Also, the aggregate 'T_m' value of ~50°C measured for antiparallel triplex–nanoparticle aggregates is lower than the value of 60°C measured for melting of parallel triplex–nanoparticle aggregates, consistent with the known comparative stability of antiparallel triplexes (34,35). Thus we have provided a simple method for examination of the melting behaviour of both parallel and antiparallel triplexes.

If triplexes are to be useful in DNA sequencing, gene control, gene therapy, etc., it is important that they form stable triplexes at physiological pH. Many research groups have targeted this problem through, for example, inclusion of chemically modified nucleobases in the third strand (36), addition of spermine to the triplex solution (37,38), covalent attachment of spermine to the oligonucleotide (39) or through the incorporation of 8-aminopurines into the hairpin strand (40–42). Recently we have shown that inclusion of 8-aminoguanine in the hairpin strand stabilizes parallel triplexes (40–42). Also, we have shown that by using hairpins carrying the purine strand linked to the Hoogsteen strand it was possible to observe a triplex to single strand transition and measure melting temperatures for this transition in antiparallel triplexes (43). In this way we demonstrated that 8-aminoguanine stabilizes antiparallel triplexes (by ~2–3°C per substitution). However, while this data applies only to triplex to single strand transitions, neither observation nor analysis of the triplex to duplex transition in 8-aminoguanine-stabilized

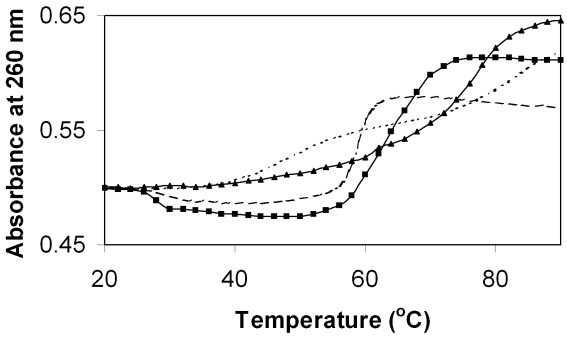

Figure 4. Normalized thermal dissociation curves for (black triangle) modified parallel triplexes formed from the hairpin h_{26}3AG5′-SH and the oligonucleotide Hoog–CT 3′-SH and for (black square) parallel triplex–nanoparticle aggregates formed using oligonucleotide–nanoparticle conjugates based on the same sequences. Also shown for comparison is the melting data of Figure 2 for (dots) unmodified parallel triplexes and for (dashes) parallel triplex–nanoparticle aggregates.

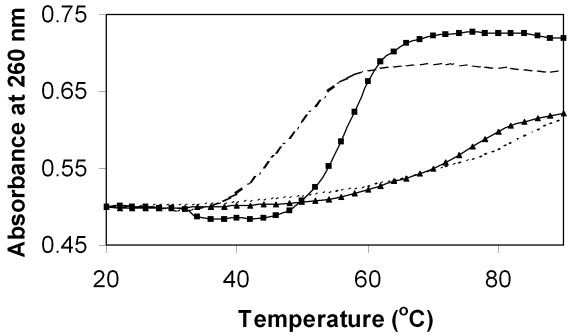

Figure 5. Normalized thermal dissociation curves for (black triangle) modified antiparallel triplexes formed from the hairpin h263AG5′-SH and the oligonucleotide Hoog-GA5′-SH and for (black square) antiparallel triplex–nanoparticle aggregates formed using oligonucleotide–nanoparticle conjugates based on the same sequences. Also shown for comparison is the melting data of Figure 3 for (dots) unmodified antiparallel triplexes and for (dashes) antiparallel triplex–nanoparticle aggregates.

antiparallel triplexes has yet been possible. To address this challenge, we employed oligonucleotide–nanoparticle conjugates to monitor the denaturation of parallel and antiparallel triplexes incorporating 8-aminoguanine nucleobases in the hairpin strand. To this end, oligonucleotide h_{26}3AG5′-SH carrying three 8-aminoguanines was prepared using standard methods (see Fig. 1, 5′-thiol-hexyl-GAAG**G**A**G**GA**G**A-TTTT-TCTCCTCCTTC-3′, where **G** = 8-aminoguanine).

Parallel triplexes were formed using oligonucleotides h_{26}3AG5′-SH and Hoog-CT3′-SH in a citrate:phosphate buffer at pH 5.5. Denaturation of this triplex was then performed and monitored via temperature-dependent UV-visible absorption spectroscopy. The derived melting curve exhibits only one transition, the duplex to random coil transition (with a T_m of ~80°C) (see Fig. 4). Also shown for comparison is the melting curve for the parallel triplex without 8-aminoguanine inclusion (data taken from Fig. 2). For 8-aminoguanine-stabilized parallel triplexes, the triplex to duplex transition is obscured by the duplex to random coil transition due to strong triplex stabilization following incorporation of 8-aminoguanine nucleobases. This is in agreement with previously observed stabilization of parallel triplexes induced by inclusion of 8-aminoguanine (>5°C per substitution) (40).

Parallel triplex–nanoparticle aggregates were then prepared by conjugating h_{26}3AG5′-SH and Hoog-CT3′-SH with gold nanoparticles via their thiol moieties. The oligonucleotide–nanoparticle conjugates were mixed together in the appropriate hybridization solution to facilitate triplex formation. As with other oligonucleotide–nanoparticle conjugate hybridizations the solution changed to a blue/black colour as the hybridization progressed, due to the formation of 3-dimensional networks of linked nanoparticles. This solution was heated under standard denaturation conditions. The resultant melting curve, obtained from UV-visible analysis, exhibits a sharp, well-defined (triplex to duplex) transition with a 'T_m' of ~65°C (see Fig. 4). The melting curve for parallel triplex–nanoparticle aggregates without incorporated 8-aminoguanine groups is also shown in Figure 4 (data taken from Fig. 2). Both of these melting curves show triplex to duplex transitions and a comparison between them clearly indicates the higher stability of triplexes that incorporate 8-aminoguanine groups.

Finally, in order to study the effect of substitution of three guanine bases by three 8-aminoguanine groups on antiparallel triplex behaviour, appropriate triplexes were prepared using h_{26}3AG5′-SH and Hoog-GA5′-SH (see Fig. 1). As this is an antiparallel triplex, a citrate:phosphate buffer at pH 7 was used as the hybridization medium. Denaturation of the triplex was monitored using temperature-dependent UV-visible absorption spectroscopy and the resulting melting curve is shown in Figure 5. This melting curve exhibits only one transition with a 'T_m' of ~80°C. Also shown in Figure 5 is the melting curve for the analogous antiparallel triplex without 8-aminoguanine incorporation (data taken from Fig. 3). For both types of triplex it was only possible to monitor denaturation of the hairpin (i.e. duplex to single strand), indicating that duplexes that incorporate 8-aminoguanine are possibly only a few degrees less stable than those that do not. This is in accordance with previous observations (40,43). Therefore, since the absorbance changes are very small and the transitions are quite broad, it is impossible to ascertain with certainty the effect of 8-aminoguanine inclusion in antiparallel triplexes using this approach.

Antiparallel triplex–nanoparticle aggregates formed using oligonucleotides incorporating 8-aminoguanine groups were then prepared using oligonucleotide–nanoparticle conjugates of the sequences h_{26}3AG5′-SH and Hoog-GA5′-SH. The triplex–nanoparticle aggregate solution was denatured under standard conditions and the resultant melting curve, obtained from UV-visible analysis, exhibits one (triplex to duplex) transition with a 'T_m' of ~60°C (see Fig. 5). The melting curve for antiparallel triplex–nanoparticle aggregates without 8-aminoguanine inclusion is also shown in Figure 5 (data taken from Fig. 3). Both of these melting curves show triplex to duplex transitions and a comparison between them clearly indicates the higher stability of antiparallel triplex–nanoparticle aggregates incorporating 8-aminoguanine groups (~10°C). This confirms the triplex stabilization properties of 8-aminoguanine observed using a more complex method in previous work using oligonucleotide hairpins (43). Therefore,

the method described here is a very useful technique for determining the binding properties of new oligonucleotide derivatives with enhanced triplex stability.

Overall, the advantages of oligonucleotide–gold nanoparticle conjugates for monitoring triplex denaturation behaviour are: (i) triplex to duplex melting transitions may be monitored for both parallel and antiparallel triplexes; (ii) the duplex to single strand transition does not significantly contribute to the measured signal; (iii) sensitivity is increased (0.32 nmol each oligonucleotide are needed for gold nanoparticle assays versus 1.5 nmol each oligonucleotide without nanoparticles); (iv) the comparative sequence-dependent stability of triplexes may be readily assessed. Specific observations concerning the denaturation behaviour and comparative stability of DNA triple helices that have been made using the oligonucleotide–nanoparticle method are: (i) triplex–nanoparticle aggregates exhibit higher thermal stability than unmodified triplexes; (ii) parallel triplexes are thermally more stable with respect to the triplex to duplex transition at pH 5.5 than antiparallel triplexes at pH 7; (iii) triplex to duplex melting transitions for parallel and antiparallel triplexes incorporating 8-aminoguanine groups may also be successfully monitored; (iv) dramatic stabilization of parallel and antiparallel triplexes following incorporation of these 8-aminopurines is confirmed.

CONCLUSION

In conclusion, we have shown that gold nanoparticles bearing oligonucleotides are valuable tools that enable characterization of DNA triplex denaturation processes. For the first time, both parallel and antiparallel triplex melting transitions can be monitored using UV-visible absorption spectroscopy. Triplex–nanoparticle aggregates exhibit sharper and better-defined melting transitions than unmodified oligonucleotides. In particular, for the first time the triplex to duplex transition of antiparallel triplexes may be readily observed. We have also demonstrated that this method can be used to assess the influence of sequence modifications on triplex behaviour; substitution of three guanines by three 8-aminoguanine groups was clearly shown to stabilize both parallel and antiparallel triplexes. As interest in the use of triplex complexes for biological applications grows, availability of a simple, easily monitored, accurate method of investigating triple helix melting characteristics and comparative stabilities will be essential. Our results may also be of use in the development of novel triplex-forming oligonucleotides and for the detection of specific nucleic acid sequences by triplex formation.

ACKNOWLEDGEMENTS

This work was supported by the Commission of the European Unions as part of the Information Societies Technology Programme (IST-1999-11974), by the HEA PRTLI1 Nanoscale Science and Technology Initiative, by the Dirección General de Investigación Científica (BQU2000-0649 and BQU2003-00397) and by The Generalitat de Catalunya (2001-SGR-0049).

REFERENCES

1. Thuong,N.T. and Hélène,C. (1993) Sequence-specific recognition and modification of double-helical DNA by oligonucleotides. *Angew. Chem. Int. Ed. Engl.*, **32**, 666–690.
2. Chan,P.P. and Glazer,P.M. (1997) Triplex DNA: fundamentals, advances and potential applications for gene therapy. *J. Mol. Med.*, **75**, 267–282.
3. Dagle,J.M. and Weeks,D.L. (1996) Positively charged oligonucleotides overcome potassium-mediated inhibition of triplex DNA formation. *Nucleic Acids Res.*, **24**, 2143–2149.
4. Escudé,E., Giovannangeli,C., Sun,J.-S., Lloyd,D.H., Chen,J.-K., Gryaznov,S.M., Garestier,T. and Hélène C. (1996) Stable triple helices formed by oligonucleotide N3′→P5′ phosphoramidates inhibit transcription elongation. *Proc. Natl Acad. Sci. USA*, **93**, 4365–4369.
5. Goobes,R., Cohen,O. and Minsky,A. (2002) Unique condensation patterns of triplex DNA: physical aspects and physiological implications. *Nucleic Acids Res.*, **30**, 2154–2161.
6. Soyter,V.N. and Potoman,V.N. (1996) *Triple-helical Nucleic Acids*. Springer-Verlag, New York, NY.
7. Benight,A.S., Pancoska,P., Owczarzy,R., Vallone,P.M., Nesetril,J. and Ricelli,P.V. (2001) Calculating sequence-dependent melting stability of duplex DNA oligomers and multiplex sequence analysis by graphs. *Methods Enzymol.*, **340**, 165–192.
8. Jetter,M.C. and Hobbs,F.W. (1993) 7,8-Dihydro-8-oxoadenine as a replacement for cytosine in the third strand of triple helixes. Triplex formation without hypochromicity. *Biochemistry*, **32**, 3249–3254.
9. Faucon,B., Mergny,J.L. and Hélène,C. (1996) Effect of third strand composition on the triple helix formation: purine versus pyrimidine oligodeoxynucleotides. *Nucleic Acids Res.*, **24**, 3181–3188.
10. Darby,R.A.J., Sollogoub,M., McKeen,C., Brown,L., Risitano,A., Brown,N., Barton,C., Brown,T. and Fox,K.R. (2002) High throughput measurement of duplex, triplex and quadruplex melting curves using molecular beacons and a LightCycler. *Nucleic Acids Res.*, **30**, e39.
11. Mirkin,C.A., Letsinger,R.L., Mucic,R.C. and Storhoff,J.J. (1996) A DNA-based method for rationally assembling nanoparticles into macroscopic materials. *Nature*, **382**, 607–609.
12. Alivisatos,A.P., Johnsson,K.P., Peng,X., Wilson,T.E., Loweth,C.J., Bruchez,M.P. and Schultz,P.G. (1996) Organization of 'nanocrystal molecules' using DNA. *Nature*, **382**, 609–612.
13. Mucic,R.C., Storhoff,J.J., Mirkin,C.A. and Letsinger,R.L. (1998) DNA-directed synthesis of binary nanoparticle network materials. *J. Am. Chem. Soc.*, **120**, 12674–12675.
14. Taton,T.A., Mucic,R.C., Mirkin,C.A. and Letsinger,R.L. (2000) The DNA-mediated formation of supramolecular mono- and multilayered nanoparticle structures. *J. Am. Chem. Soc.*, **122**, 6305–6306.
15. Loweth,C.J., Caldwell,W.B., Peng,X., Alivisatos,A.P. and Schultz,P.G. (1999) DNA-based assembly of gold nanocrystals. *Angew. Chem. Int. Ed. Engl.*, **38**, 1808–1812.
16. Elghanian,R., Storhoff,J.J., Mucic,R.C., Letsinger,R.L. and Mirkin,C.A. (1997) Selective colorimetric detection of polynucleotides based on the distance-dependent optical properties of gold nanoparticles. *Science*, **277**, 1078–1081.
17. Storhoff,J.J., Elghanian,R., Mucic,R.C., Mirkin,C.A. and Letsinger,R.L. (1998) One-pot colorimetric differentiation of polynucleotides with single base imperfections using gold nanoparticle probes. *J. Am. Chem. Soc.*, **120**, 1959–1964.
18. Reynolds,R.A., Mirkin,C.A. and Letsinger,R.L. (2000) Homogeneous, nanoparticle-based quantitative colorimetric detection of oligonucleotides. *J. Am. Chem. Soc.*, **122**, 3795–3796.
19. Letsinger,R.L., Elghanian,R., Viswanadham,G. and Mirkin,C.A. (2000) Use of a steroid cyclic disulfide anchor in constructing gold nanoparticle-oligonucleotide conjugates. *Bioconjugate Chem.*, **11**, 289–291.
20. Storhoff,J.J. and Mirkin,C.A. (1999) Programmed materials synthesis with DNA. *Chem. Rev.*, **99**, 1849–1862.
21. Park,S.J., Lazarides,A.A., Mirkin,C.A., Brazis,P.W., Kannewurf,C.R. and Letsinger,R.L. (2000) The electrical properties of gold nanoparticle assemblies linked by DNA. *Angew. Chem. Int. Ed. Engl.*, **39**, 3845–3848.
22. Hayat,M.A. (1991) *Collidal Gold: Principles*, *Methods and Applications*. Academic Press, San Diego, CA.
23. Grabar,K.C., Freeman,R.G., Hommer,M.B. and Natan,M.J. (1995) Preparation and characterization of Au colloid monolayers. *Anal. Chem.*, **67**, 735–743.
24. Rao,T.S., Durland,R.H. and Revankar,G.R. (1994) Synthesis of oligonucleotides containing 7-(2-deoxy-β-D-*erythro*-

pentofuranosyl)guanine and 8-amino-2′-deoxyguanosine. *J. Heterocyclic Chem.*, **31**, 935–940.
25. Rieger,R.A., Iden,C.R., Gonikberg,E. and Johnson,F. (1999) 8-Amino-2′-deoxyguanosine incorporation into oligomeric DNA. *Nucl. Nucl.*, **18**, 73–88.
26. Taton,T.A. (2002) Preparation of gold nanoparticle-DNA conjugates. In *Current Protocols in Nucleic Acid Chemistry*. John Wiley & Sons, New York, NY, Ch. 12.2.1–12.2.11.
27. Demers,L.M., Mirkin,C.A., Mucic,R.C., Reynolds,R.A., Letsinger,R.L., Elghanian,R. and Viswanadham,G. (2000) A fluorescence-based method for determining the surface coverage and hybridization efficiency of thiol-capped oligonucleotides bound to gold thin films and nanoparticles. *Anal. Chem.*, **72**, 5535–5541.
28. Manzini,G., Xodo,L.E., Gasparotto,D., Quadrifoglio,F., Vandermarel,G.A. and Vanboom,J.H. (1990) Triple helix formation by oligopurine-oligopyrimidine DNA fragments—electrophoretic and thermodynamic behaviour. *J. Mol. Biol.*, **213**, 833–843.
29. He,Y., Scaria,P.V. and Shafer,R.H. (1997) Studies on formation and stability of the d[G(AG)(5)]*d[G(AG)(5)]·d[C(TC)(5)] and d[G(TG)(5)]*d[G(AG)(5)]·d[C(TC)(5)] triple helices. *Biopolymers*, **41**, 431–441.
30. Mills,M., Arimondo,P.B., Lacroix,L., Garestier,T., Klump,H. and Mergny,J.-L. (2002) Chemical modification of the third strand: differential effects on purine and pyrimidine triple helix formation. *Biochemistry*, **41**, 357–366.
31. Ji,J., Hogan,M.E. and Gao,X. (1996) Solution structure of an antiparallel purine motif triplex containing a T·CG pyrimidine base triple. *Structure*, **4**, 425–435.
32. Radhakrishnan,I. and Patel,D.J. (1993) Solution structure of a purine purine pyrimidine DNA tripler containing G·GC and T·AT triples. *Structure*, **1**, 135–152.
33. Jaumot,J., Aviñó,A., Eritja,R., Tauler,R. and Gargallo,R. (2003) Resolution of parallel and antiparallel oligonucleotide triple helices formation and melting processes by multivariate curve resolution. *J. Biomol. Struct. Dyn.*, **21**, 267–279.
34. Cheng,Y.-K. and Pettitt,B.M. (1992) Hoogsteen versus reversed-Hoogsteen base pairing: DNA triple helixes *J. Am. Chem. Soc.*, **114**, 4465–4474.
35. Chandler,S.P. and Fox,K.R. (1996) Specificity of antiparallel triple helix formation. *Biochemistry*, **35**, 15038–15048.
36. Xodo,L.E., Manzini,G., Quadrifoglio,F., van der Marel,G.A. and van Boom,J.H. (1991) Effect of 5-methylcytosine on the stability of triple-stranded DNA—a thermodynamic study. *Nucleic Acids Res.*, **19**, 5625–5631.
37. Volker,J. and Klump,H.H. (1994) Electrostatic effects in DNA triple helixes. *Biochemistry*, **33**, 13502–13508.
38. Thomas,T. and Thomas,T.J. (1993) Selectivity of polyamines in triplex DNA stabilization. *Biochemistry*, **32**, 14068–14074.
39. Rajeev,K.G., Jadhav,V.R. and Ganesh,K.N. (1997) Triplex formation at physiological pH: comparative studies on DNA triplexes containing 5-Me-dC tethered at N^4 with spermine and tetraethyleneoxyamine. *Nucleic Acids Res.*, **25**, 4187–4193.
40. Soliva,R., Güimil-García,R., Blas,J.R., Eritja,R., Asensio,J.L., González,C., Luque,F.J. and Orozco,M. (2000) DNA-triplex stabilizing properties of 8-aminoguanine. *Nucleic Acids Res.*, **28**, 4531–4539.
41. Güimil-García,R., Bachi,A., Eritja,R., Luque,F.J. and Orozco,M. (1998) Triple helix stabilization properties of oligonucleotides containing 8-amino-2′-deoxyguanosine. *Bioorg. Med. Chem. Lett.*, **8**, 3011–3016.
42. Aviñó,A., Frieden,M., Morales,J.C., de la Torre,B.G., Güimil-García,R., Azorín,F., Gelpí,J.L., Orozco,M., González,C. and Eritja,R. (2002) Properties of triple helices formed by parallel-stranded hairpins containing 8-aminopurines. *Nucleic Acids Res.*, **30**, 2609–2619.
43. Aviñó,A., Cubero,E., González,C., Eritja,R. and Orozco,M. (2003) Antiparallel triple helices. Structural characteristics and stabilization by 8-amino derivatives. *J. Am. Chem. Soc.*, **125**, 16127–16138.